JVST A
Journal of Vacuum Science & Technology A

ARTICLE

avs.scitation.org/journal/jva

Thermal atomic layer etching of cobalt using sulfuryl chloride for chlorination and tetramethylethylenediamine or trimethylphosphine for ligand addition

Cite as: J. Vac. Sci. Technol. A **41**, 032603 (2023); doi: 10.1116/6.0002488
Submitted: 14 January 2023 · Accepted: 15 March 2023 ·
Published Online: 25 April 2023

View Online Export Citation CrossMark

Jessica A. Murdzek, Ann Lii-Rosales, and Steven M. George[a)]

AFFILIATIONS

Department of Chemistry, University of Colorado Boulder, Boulder, Colorado 80309-0215

Note: This paper is part of the 2024 Special Topic Collection on Atomic Layer Etching (ALE).

[a)]**Author to whom correspondence should be addressed:** Steven.George@Colorado.edu

ABSTRACT

Thermal atomic layer etching (ALE) of cobalt was developed using sulfuryl chloride (SO_2Cl_2) for chlorination and either tetramethylethylenediamine (TMEDA) or trimethylphosphine (PMe_3) for ligand addition. *In situ* quartz crystal microbalance (QCM) measurements were used to monitor the thermal ALE of cobalt using the SO_2Cl_2/TMEDA and SO_2Cl_2/PMe_3 processes. For every SO_2Cl_2 exposure, there was a mass gain during chlorination. For every TMEDA or PMe_3 exposure, there was a mass loss during ligand addition. The result was a net removal of cobalt during each chlorination/ligand-addition reaction cycle. Average etch rates determined from QCM measurements for the SO_2Cl_2/TMEDA process at 175, 200, 225, 250, 275, and 300 °C were 0.62 ± 0.41, 1.35 ± 0.64, 2.31 ± 0.91, 6.43 ± 1.31, 10.56 ± 2.94, and 7.62 ± 4.87 Å/cycle, respectively. These etch rates were corroborated using x-ray reflectivity (XRR) studies on cobalt thin films on silicon coupons. Quadrupole mass spectroscopy analysis also revealed that the cobalt etch product from TMEDA exposures on $CoCl_2$ powder was $CoCl_2$(TMEDA). The SO_2Cl_2/TMEDA process could remove the surface chloride layer formed by each SO_2Cl_2 exposure with one TMEDA exposure. In contrast, the SO_2Cl_2/PMe_3 process required 20–40 individual PMe_3 exposures to remove the surface chloride layer formed from each SO_2Cl_2 exposure at 130–200 °C. An increasing number of PMe_3 exposures were needed as the temperature decreased below 130 °C. The etch rates for the SO_2Cl_2/PMe_3 process with multiple PMe_3 exposures were 2–4 Å/cycle as determined by the QCM and XRR studies. For both the SO_2Cl_2/TMEDA and SO_2Cl_2/PMe_3 processes, the etch rate was determined by the amount of $CoCl_2$ created during the SO_2Cl_2 exposure. Thicker surface $CoCl_2$ layers from larger SO_2Cl_2 exposures resulted in higher Co etch rates that could exceed one crystalline unit cell length. Atomic force microscopy measurements determined that the cobalt surface roughness decreased after Co ALE with the SO_2Cl_2/TMEDA process. In contrast, the cobalt surface roughness increased after Co ALE with the SO_2Cl_2/PMe_3 process. The chlorination and ligand-addition mechanism should be generally applicable for metal ALE for metals that form stable chlorides.

I. INTRODUCTION

Thermal atomic layer etching (ALE) is typically comprised of two sequential reactions: surface modification and volatile release.[1,2] Thermal ALE can be viewed as the opposite of atomic layer deposition (ALD).[3,4] During thermal ALE, the surface modification step involves a reaction that alters the top surface layer.[1,2] The removal step then exposes the modified surface to a precursor that will form stable, volatile species with the modified surface. Thermal ALE produces isotropic etching because both sequential reactions are initiated by the flux resulting from the pressure of gas phase reactants.[5,6] Thermal ALE complements plasma ALE techniques that produce anisotropic etching by employing directional energetic ions for the release of the etch products through sputtering.[7]

Materials that have been etched with thermal ALE include many metal oxides, such as Al_2O_3, HfO_2, and ZrO_2.[5,8–14] These metal oxides are etched using fluorination as the surface modification step and ligand-exchange for the volatile release step. A typical etch rate is 0.51 Å/cycle for Al_2O_3 ALE using HF and trimethylaluminum (TMA) at 300 °C.[11] Another thermal ALE mechanism can involve conversion reactions that convert the initial surface material to a different material.[15] These conversion reactions have successfully etched a variety of materials such as SiO_2 and WO_3.[16,17] A typical etch rate is 4.18 Å/cycle for WO_3 ALE using BCl_3 and HF at 207 °C.[17] Oxidation reactions, sometimes together with conversion reactions, have also been employed for the etching of many materials such as W, TiN, Si, Si_3N_4, and SiGe.[17–21]

In contrast to the previous work for the thermal ALE of oxides and nitrides, few metals have been etched using thermal ALE. Thermal ALE of metals can be difficult because the modification step must also change the oxidation state of the metal surface. This change in the oxidation state is needed because volatile metal species usually contain the metal in an oxidized state. The change in the oxidation state can be accomplished by (1) oxidation to create a metal oxide layer, (2) chlorination to create a metal chloride layer, or (3) fluorination to create a metal fluoride layer. After the oxidation state of the metal has been changed, different precursors can be used to form stable and volatile species via different types of reactions.

Cu thermal ALE has been performed using oxidation as the first reaction, followed by a second reaction using hexafluoroacetylacetonate (hfacH).[22] During this hfacH reaction, the ligand addition of hfac and hydrogen transfer to the copper oxide form Cu$(hfac)_2$ and H_2O as by-products.[22] Co thermal ALE has also been demonstrated by chlorination as the first reaction, and then ligand addition and hydrogen-transfer reactions using hfacH as the second reaction.[23,24] Co$(hfac)_2$ and HCl are believed to be the etching products.[24] Thermal cycling Co ALE methods have also been developed involving plasma oxidation at a low temperature of 25°C and then thermal annealing to a higher temperature of 210 °C in the presence of acetylacetone (acacH).[25]

Ligand addition without hydrogen transfer has also been used as the volatile release step for thermal Ni ALE.[26] The thermal Ni ALE process involves chlorination using SO_2Cl_2 to create $NiCl_2$ surface species. The ligand-addition step is then defined by exposure to PMe_3 ligands that bind to and volatilize the $NiCl_2$ surface species.[26] The PMe_3 ligands add directly to the $NiCl_2$ surface species to form the etch products. A typical etch rate is 1.97 Å/cycle for Ni ALE using SO_2Cl_2 and PMe_3 at 175 °C.[26] The etch product observed by quadrupole mass spectrometry (QMS) studies was $NiCl_2(PMe_3)_2$.[26]

The Co thermal ALE process developed in this work follows the mechanism shown in Fig. 1. For the surface modification step, the Co surface is exposed to sulfuryl chloride (SO_2Cl_2) and forms a $CoCl_2$ surface layer. The volatile release step involves exposing the $CoCl_2$ surface layer to a ligand-addition precursor. This ligand-addition precursor is denoted as "L" in Fig. 1.[27] The ligand addition leads to the formation of a volatile $CoCl_xL_y$ species. The L ligands were tetramethylethylenediamine (TMEDA) and PMe_3. TMEDA is a bidentate ligand where the two electron lone pairs on the two nitrogen atoms bind to the metal center. PMe_3 is a monodentate ligand where the electron lone pair on phosphorous binds to the metal center.

Cobalt etching is necessary for the fabrication of magnetic devices such as magnetic tunneling junctions for magnetic random access memory.[28,29] Cobalt etching is also important for cobalt recess etching for advanced interconnects.[30] Cobalt can be etched using wet etching techniques using HCl or H_3PO_4 acid solutions.[31] Another wet etch approach is to first oxidize cobalt in a H_2O_2 solution. Subsequently, the passivating cobalt oxide layer can be dissolved in dilute HF.[30] Cobalt has also been shown to etch in a solution of hfacH or acacH.[28] Unfortunately, wet etching rates are usually high and not precise at the atomic level.

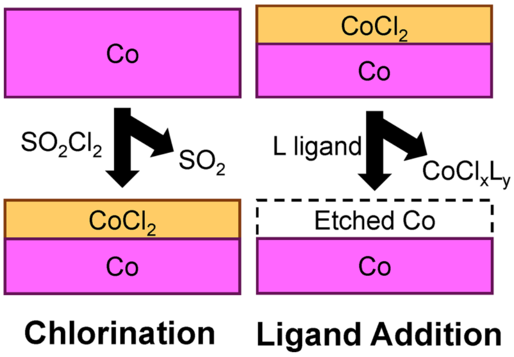

FIG. 1. Proposed mechanism for Co ALE using SO_2Cl_2 for chlorination and an L ligand for ligand-addition to produce a volatile $CoCl_xL_y$ etch species.

Cobalt can also be etched in vacuum using ion-based techniques. For example, a two-step process defined by acacH exposure and an Ar ion beam exposure leads to Co volatilization.[28] This two-step process has a reported etch rate of 13 Å/min. In comparison, the Ar ion beam sputtering alone led to an etch rate of 7 Å/min.[28] This ion beam-assisted cobalt etching is more controllable than the solution etching processes. However, the Ar ion beam is directional and does not produce isotropic etching. In addition, the Ar ion beam can lead to the undesirable damage of the cobalt surface and near-surface region.

This study focused on Co thermal ALE using chlorination with SO_2Cl_2 and ligand addition with either TMEDA or PMe_3. Co etch rates were measured with quartz crystal microbalance (QCM) or x-ray reflectivity (XRR) measurements. The temperature dependence of Co thermal ALE was explored using both TMEDA and PMe_3. QMS was utilized to identify the volatile etch species. Atomic force microscopy was also employed to study the roughness of the surface after Co thermal ALE.

II. EXPERIMENT

A. Reactor and *in situ* QCM measurements

Thermal ALE experiments were performed in a viscous flow reactor.[32] The reaction temperatures were maintained by a proportional-integral-derivative temperature controller (2604, Eurotherm). A constant flow of ultrahigh purity (99.999%) Ar gas was employed as the carrier and purge gas using mass flow controllers (type 1179A, MKS). A mechanical pump (Pascal 2015SD, Alcatel) was attached at the back of the reactor. The reactor pressure with flowing Ar carrier gas was 1 Torr. This pressure was measured by a capacitance manometer (Baratron 121A, MKS).

QCM studies were performed in the viscous flow reactor.[32] The quartz crystals (polished, RC cut, 6 MHz, Phillip Technologies) were coated with ∼2000 Å of sputtered cobalt. The cobalt-coated crystal was placed in a sensor head (Inficon) and sealed with a high temperature silver epoxy (Epo-Tek H21D, Epoxy Technology Inc.).

The QCM head was placed in an isothermal region of the reactor. A constant argon gas flow on the back of the QCM was used to prevent the interaction of precursors with the backside of the QCM crystal.[32] The changes in the resonant frequency of the quartz crystal were recorded and converted to mass using a thin film deposition monitor (Maxtek TM-400, Inficon). The QCM has a precision of ∼1 ng/cm^2. The cobalt-coated crystal was maintained in the reactor at temperature to equilibrate for at least 6 h before starting the experiments.

B. Co films for *ex situ* XRR experiments

Cobalt thin films were prepared using physical vapor deposition on thermal SiO_2 on a silicon substrate. These cobalt films were prepared by Intel. The cobalt wafer was cut into 2×2 cm^2 pieces to fit in the reactor. These cobalt films were polycrystalline with a hexagonal structure as verified with grazing incidence x-ray diffraction (GI-XRD). These cobalt films had a thickness of 120–140 Å and a native oxide (CoO) layer on top of the cobalt with a thickness of ∼60–70 Å according to x-ray reflectivity (XRR) analysis.

Both GI-XRD and XRR scans were performed using an XRD instrument (Bede D1, Jordan Valley Semiconductors) with radiation from Cu Kα ($\lambda = 1.540$ Å). The x-ray tube filament voltage was 40 kV, and the current was 35 mA. The incident angle used for the GI-XRD measurements was 0.3°. The XRR scan range was 300–6000 arcsec with a 5 arcsec step size. The XRR scans were analyzed using modeling software (REFS, Jordan Valley Semiconductors).

C. Reactants in viscous flow reactor and AFM measurements

Each reagent was dosed into the constant stream of Ar carrier gas in the viscous flow reactor. The chlorination precursor was sulfuryl chloride (SO_2Cl_2, 97%, Sigma-Aldrich). Sulfuryl chloride is a liquid with high vapor pressure that is easily handled in the laboratory.[33] SO_2Cl_2 will also thermally decompose to $SO_2 + Cl_2$ at temperatures approaching 300 °C and higher.[34] The pressure transients during the SO_2Cl_2 exposures were 100 m Torr. These pressures were defined by a metering valve (SS-4BMG, Swagelok). The ligand-addition precursors were tetramethylethylenediamine (TMEDA, 99.5%, Sigma-Aldrich) and trimethylphosphine (PMe_3, 97%, Sigma-Aldrich). Pressure transients were 40 m Torr for TMEDA exposures and 300 m Torr for PMe_3 exposures. These pressure transients were also controlled by metering valves.

The thermal Co ALE experiments were performed with an exposure of 1 s for all precursors (SO_2Cl_2, TMEDA, and PMe_3). The Ar purge times were determined by the time required for the mass change to level out after the precursor exposure. The Ar purge time was between 60 and 200 s after the SO_2Cl_2 exposure. The purge time was between 60 and 120 s following the PMe_3 exposures. The longer purge times were employed at lower temperatures. At 70 °C, the purge times were 200 s after the SO_2Cl_2 exposures and 300 s following the PMe_3 exposures. At 80–100 °C, the purge times were 200 s after the SO_2Cl_2 exposures and 120 s following the PMe_3 exposures. At 110–130 °C, the purge times were 120 s after the SO_2Cl_2 exposures and 90 s following the PMe_3 exposures. At 140–200 °C, the purge times were 120 s after the SO_2Cl_2 exposures and 60 s following the PMe_3 exposures. The purge times were 120 s after the SO_2Cl_2 exposures and 300 s following the TMEDA exposures at 175–300 °C.

For the experiments using SO_2Cl_2 and TMEDA, the reaction sequence for one cycle was one exposure of SO_2Cl_2 followed by one exposure of TMEDA. When using SO_2Cl_2 and PMe_3, one cycle consisted of one exposure of SO_2Cl_2 followed by a number of individual PMe_3 exposures (x), where x was variable and optimized for each temperature. The Co and CoO thicknesses before and after the Co thermal ALE process were measured with XRR. The etch rate was determined by a comparison of the Co thicknesses before and after the Co thermal ALE.

Atomic force microscopy (AFM) was utilized to evaluate the surface of the cobalt films before and after Co thermal ALE. These AFM measurements were performed with an AFM instrument (Park NX10) using noncontact mode. The scan rate was 0.2–1.0 Hz with a microcantilever probe (Olympus OMCL-AC160TS). The average RMS roughness values were obtained using RMS roughness measurements at three different locations for each sample.

D. Quadrupole mass spectrometry experiments

Detection of volatile etch species was accomplished using quadrupole mass spectrometry (QMS).[35] The quadrupole mass spectrometer has 19 mm-diameter mass filter quadrupole poles, an operating frequency of 880 kHz, and a mass range of 1–1000 amu (Extrel, MAX-QMS Flange Mounted System). QMS acquisitions were performed in a mass-to-charge (m/z) window of 1–1000 amu using an electron ionization energy of 70 eV. Each scan from 1 to 1000 amu was completed in 2.2 s, and there were 27 data points per amu. For the temperature ramp experiments, the QMS scans were recorded throughout the temperature ramp.

The reactor and sample holder for the QMS experiments have been described previously.[35] During the QMS experiments, TMEDA at ∼0.5 Torr in a N_2 carrier gas flows through $CoCl_2$ powder (Strem Chemicals, anhydrous, 99.999%).[35] A fraction of the N_2 carrier gas, etch products, and remaining TMEDA precursor exits the sample holder through an aperture. Gas expansion through the aperture then creates a molecular beam that travels through a skimmer before arriving at the ionization region of the mass spectrometer.[35] Ionization of gas is achieved by electron-impact ionization with a circular thoriated iridium filament in the ionization volume. The QMS mass analyzer was positioned perpendicular to the incoming molecular beam to minimize exposures to corrosive gaseous species.

E. X-ray photoelectron spectroscopy

X-ray photoelectron spectroscopy (XPS) (PHI 5600, RBD Instruments) was employed to determine the film composition. A monochromatic Al K_α x-ray source (1486.6 eV) was utilized to collect survey scans with a pass energy of 93.9 eV and a step size of

0.400 eV. Casa XPS software (Casa XPS, Casa Software) determined the surface concentrations using the XPS signals and their corresponding sensitivity factors. The XPS peaks were calibrated to the C 1s peak for adventitious carbon centered at 284.8 eV.

III. RESULTS AND DISCUSSION

A. QCM measurements

1. TMEDA as ligand-addition precursor

Cobalt thermal ALE using sequential SO_2Cl_2 and TMEDA exposures was analyzed using QCM measurements. The results at 250 °C are displayed in Fig. 2. The linear mass reduction versus time for 50 cycles of Co thermal ALE with a SO_2Cl_2/TMEDA cycle time of 422 s is shown in Fig. 2(a). The mass loss of 34 500 ng/cm^2 over 50 cycles is equivalent to an average etch rate of 7.75 Å/cycle. This conversion is based on the Co density of 8.90 g/cm^3.

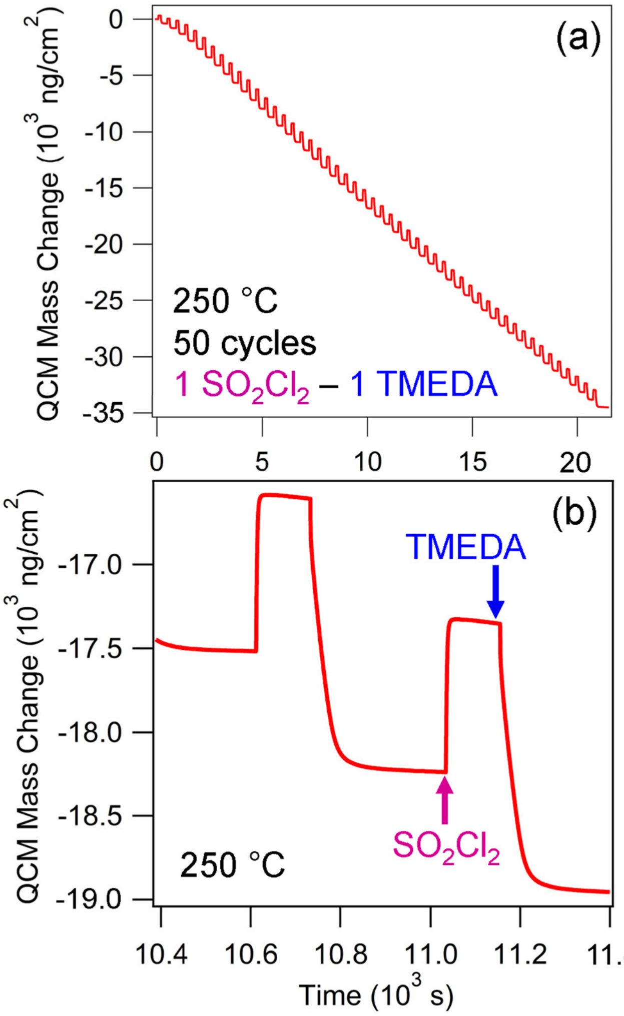

FIG. 2. (a) Mass change vs time during 50 cycles of Co ALE using SO_2Cl_2 and TMEDA as reactants at 250 °C. (b) Magnification of two Co ALE cycles in (a) showing a mass increase during single SO_2Cl_2 exposure and a mass decrease during single TMEDA exposure.

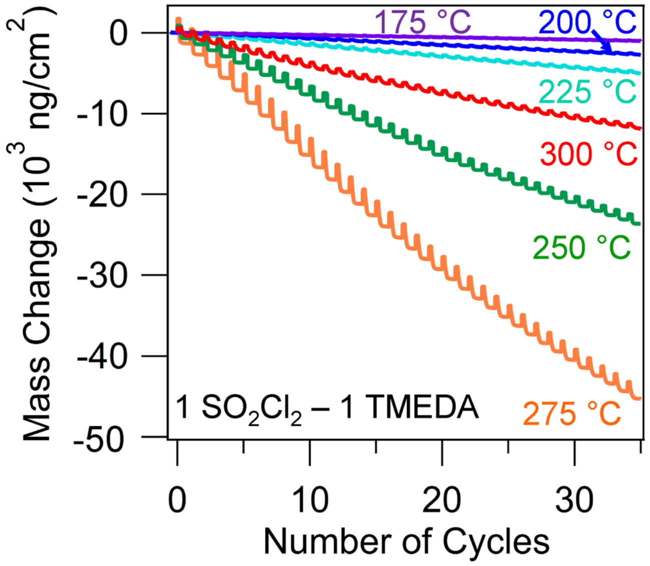

FIG. 3. Mass change vs number of ALE cycles showing 35 Co ALE cycles using SO_2Cl_2 and TMEDA as reactants at 175, 200, 225, 250, 175, and 300 °C. Pulse sequence was performed with single SO_2Cl_2 exposure and single TMEDA exposure.

Two Co thermal ALE cycles from Fig. 2(a) are expanded and displayed in Fig. 2(b) to investigate the mechanism of Co thermal ALE. On each SO_2Cl_2 exposure, the mass increases by approximately 875 ng/cm^2 as expected if SO_2Cl_2 is chlorinating the Co surface according to the reaction $Co + SO_2Cl_2(g) \rightarrow CoCl_2 + SO_2(g)$. This reaction is thermochemically favorable with a standard free energy change of ΔG° (250 °C) = −62.8 kcal.[36] The mass subsequently decreases with each TMEDA exposure. This decrease is expected if the ligand addition of TMEDA leads to the volatilization of the cobalt chloride surface layer. The volatilization reaction is believed to be $CoCl_2 + TMEDA(g) \rightarrow CoCl_2(TMEDA)(g)$. $CoCl_2$(TMEDA) is a known Co complex from the literature.[37]

QCM results at various temperatures for 35 cycles of Co thermal ALE using SO_2Cl_2 and TMEDA as the reactants are shown in Fig. 3. The lowest etch rate is 0.33 Å/cycle at 175 °C. The highest etch rate is 14.54 Å/cycle at 275 °C. In comparison, the unit cell length for crystalline h-Co is 4.07 Å along the c-axis. The etch rates for the 35 cycles shown at 200, 225, 250, and 300 °C are 0.88, 1.62, 7.59, and 3.80 Å/cycle, respectively. Note that the etch rate at 300 °C was lower than the etch rate at 275 °C.

The average etch rates from multiple Co ALE experiments using QCM experiments with SO_2Cl_2 and TMEDA as the reactants are shown in Fig. 4. At least three separate experiments were performed at each temperature. The error bars reflect the variation

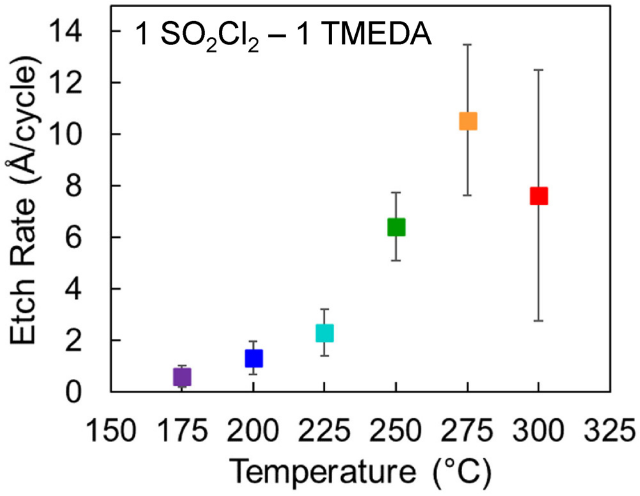

FIG. 4. Etch rates at various temperatures for Co ALE determined from QCM measurements using SO_2Cl_2 and TMEDA as reactants.

between the different QCM experiments. This variation from experiment to experiment can be partially attributed to the order of experiments and different QCM units.

The etch rates increase with increasing temperature until 275 °C. Subsequently, the average etch rate decreases at 300 °C. The variation between various individual experimental results also increases dramatically at 300 °C. Possible reasons for this large variation and decreased average etch rate at 300 °C could be the decomposition of the proposed $CoCl_2(TMEDA)$ etch product. The $CoCl_2(TMEDA)$ compound under 1 atm of nitrogen gas has been reported to decompose at 310–342 °C.[37] This observed decomposition temperature is close to the observed decrease in the Co thermal ALE etch rate at 300 °C. XPS investigations were performed after Co ALE at 300 °C to analyze the surface composition. Unfortunately, these XPS measurements could not distinguish between carbon decomposition products and adventitious carbon.

The QCM measurements can be used to determine how much $CoCl_2$ is created during each SO_2Cl_2 exposure and how much $CoCl_2$ is lost during each TMEDA exposure. The cobalt chlorination is analyzed assuming that all the mass gained during the SO_2Cl_2 exposure is attributed to chlorine. In addition, this chlorine is presumed to react with cobalt to form stoichiometric $CoCl_2$. Finally, the surface area of the cobalt QCM crystal is assumed to be 1 cm^2. This assumption is valid if the cobalt film is smooth and if any possible roughness adds a negligible amount to the surface area.

For the Co ALE using SO_2Cl_2/TMEDA at 250 °C shown in Fig. 2, the average mass change during the SO_2Cl_2 exposure is $\Delta m_{SO_2Cl_2} = 786.7$ ng/cm^2. This mass gain represents the addition of 786.7 ng of Cl to the 1 cm^2 surface area. This mass gain of chlorine is equivalent to the creation of 1.11×10^{-8} mol of $CoCl_2$ based on the molar ratio of 2 Cl to 1 $CoCl_2$. The mass of $CoCl_2$ formed is 1440.7 ng using the molar mass of 129.84 g/mol for $CoCl_2$. The accepted density of $CoCl_2$ is 3.36 g/cm^3. This density is used to convert the mass of $CoCl_2$ to a $CoCl_2$ thickness of 42.88 Å. This 42.88 Å of $CoCl_2$ was created from 7.36 Å of cobalt. The much larger thickness of $CoCl_2$ results from the large volume expansion during cobalt chlorination.

The average mass loss during the TMEDA exposure is $\Delta m_{TMEDA} = -1462.6$ ng/cm^2 for the 35 ALE cycles at 250 °C shown in Fig. 2. In comparison, there was an average of 1440.7 ng of $CoCl_2$ created from the previous SO_2Cl_2 exposure. The average remaining $CoCl_2$ left after the TMEDA exposure is $1440.7 - 1462.6 = -21.9$ ng. The TMEDA exposure removed slightly more mass than the $CoCl_2$ created on the previous step. This behavior may indicate that there was underlying $CoCl_2$ left over from a previous experiment that was then removed during Co ALE at 250 °C. On average, the TMEDA ligand-addition reaction removes 101.5% of the $CoCl_2$ formed from the previous SO_2Cl_2 exposure on the QCM surface at 250 °C.

The mass changes can also be analyzed for the other temperatures of 175, 200, 225, 275, and 300 °C shown in Fig. 3. The average $\Delta m_{SO_2Cl_2}$ mass gains are 43.9, 105.3, 189.3, 1607.8, and 415.9 ng/cm^2, respectively. The average Δm_{TMEDA} mass losses are −73.4, −184.7, −330.1, −2881.2, and −754.4 ng/cm^2, respectively. Based on the average $\Delta m_{SO_2Cl_2}$ mass gains and average Δm_{TMEDA} mass losses, the average percent $CoCl_2$ removed at 175, 200, 225, 275, and 300 °C are 91%, 95.8%, 95.2%, 97.9%, and 99.1%, respectively. These percentages of >90% for $CoCl_2$ removed at each temperature demonstrate that the TMEDA ligand-addition reaction is very efficient. Additional TMEDA exposures did not result in further mass loss. This behavior indicates that the TMEDA ligand-addition reaction is self-limiting.

2. PMe_3 as ligand-addition precursor

PMe_3 can also be employed as a ligand-addition precursor. The results for SO_2Cl_2 as the chlorination reactant and PMe_3 as the ligand-addition reactant are shown in Fig. 5(a) for 40 cycles of Co thermal ALE at 175 °C. The mass loss is linear versus Co ALE cycles over the range of 40 ALE cycles. The mass loss of 12 080 ng/cm^2 over 40 cycles is equivalent to an etch rate of 3.39 Å/cycle.

Two cycles of Co ALE using SO_2Cl_2 and PMe_3 as the reactants in Fig. 5(a) are expanded and displayed in Fig. 5(b). There is a mass gain when SO_2Cl_2 is exposed to the cobalt surface as expected if a $CoCl_2$ surface layer is formed during the chlorination process. Likewise, there is a mass loss when PMe_3 is exposed to the $CoCl_2$ surface to form the expected $CoCl_2(PMe_3)_2$ volatile etch product. This etch product is predicted based on earlier results for Ni thermal ALE using SO_2Cl_2 and PMe_3 as the reactants.[26]

Many PMe_3 exposures are needed to remove the $CoCl_2$ layer on the surface. Figure 5(b) reveals that 30 PMe_3 exposures are necessary at 175 °C. Each individual PMe_3 exposure results in additional mass loss. This behavior indicates that some $CoCl_2$ is removed on each PMe_3 exposure. The ligand-addition reaction of PMe_3 with $CoCl_2$ is much less favorable than the ligand-addition reaction of TMEDA with $CoCl_2$. The ligand-addition reaction of PMe_3 with $CoCl_2$ is also less favorable than the ligand-addition reaction of PMe_3 with $NiCl_2$ where one PMe_3 exposure could lead to complete removal of the $NiCl_2$ surface layer.[26]

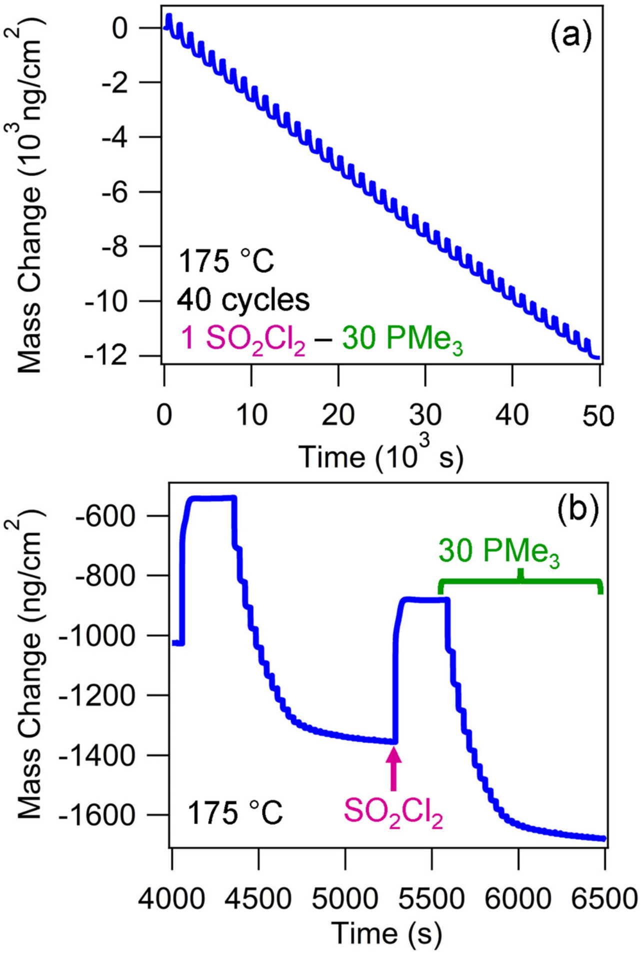

FIG. 5. (a) Mass change vs time during 40 cycles of Co ALE using SO_2Cl_2 and PMe_3 as reactants at 175 °C. (b) Magnification of two Co ALE cycles in (a) showing a mass increase during single SO_2Cl_2 exposure and a mass decrease during 30 PMe_3 exposures.

Nearly all the available $CoCl_2$ has been removed near the end of the 30 PMe_3 exposures. The last few PMe_3 exposures during each cycle in Fig. 5(b) remove very little mass. Based on the average $\Delta m_{SO_2Cl_2}$ mass gains and average Δm_{PMe_3} mass losses, the average percent $CoCl_2$ removed by the 30 PMe_3 exposures for the results in Fig. 5(b) at 175 °C is 94%.

The number of PMe_3 exposures required to remove the $CoCl_2$ layer varies greatly with temperature. Figure 6 shows the number of PMe_3 exposures per cycle needed to remove the $CoCl_2$ layer at various temperatures. For temperatures >130 °C, around 25 PMe_3 exposures are needed to remove the $CoCl_2$ layer. However, for temperatures <130 °C, the number of PMe_3 exposures required to remove the $CoCl_2$ layer dramatically increases. Almost 350 PMe_3 exposures are necessary to remove the $CoCl_2$ layer at 70 °C.

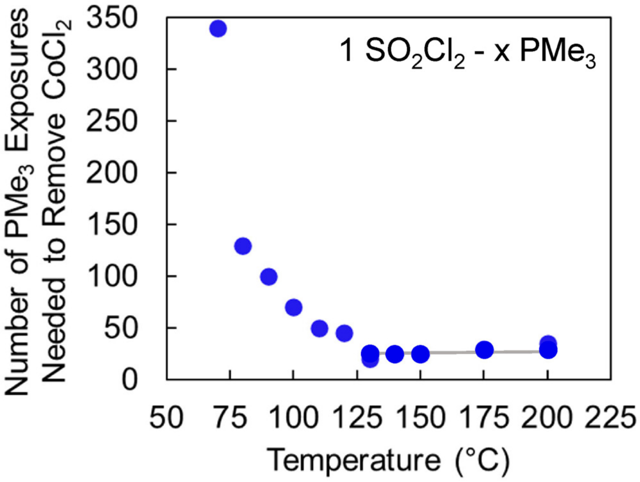

FIG. 6. Number of PMe_3 exposures in each Co ALE cycle needed to remove the $CoCl_2$ layer as a function of temperature.

The etch rates from 80 to 200 °C derived by the QCM and XRR measurements are summarized for Co ALE using SO_2Cl_2 and PMe_3 as the reactants in Fig. 7. The number of PMe_3 exposures per cycle was optimized for each temperature. The etch rates determined by the QCM and XRR techniques agree well with each other. The etch rate does not vary significantly with temperature. All the Co etch rates were between 2 and 4 Å/cycle. In addition, an average of 90%–95% of the $CoCl_2$ surface layer formed by the SO_2Cl_2 exposure was removed by the PMe_3 exposures regardless of temperature.

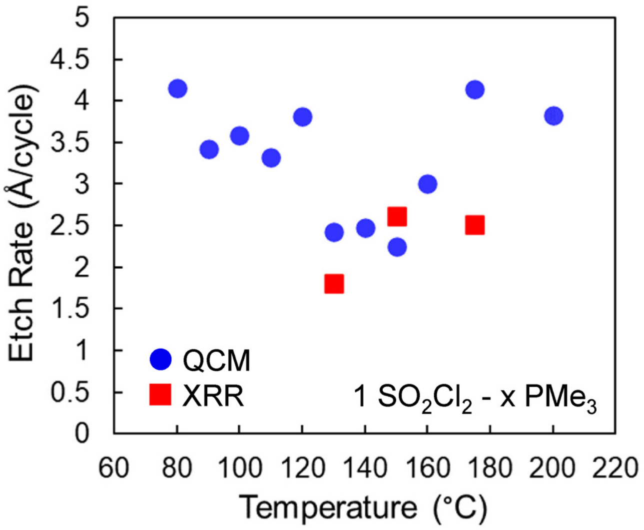

FIG. 7. Etch rate vs temperature for Co ALE using SO_2Cl_2 and PMe_3 measured by QCM (blue circles) and XRR (red squares).

B. XRR measurements on cobalt coupons

The cobalt etch rates using both TMEDA and PMe_3 as the ligand-addition precursor were also quantified using cobalt thin films prepared by physical vapor deposition on thermal SiO_2 on silicon coupons. The etch rates were determined using XRR measurements. Figure 8 shows the thickness change for the cobalt films using SO_2Cl_2 and TMEDA as the reactants at temperatures from 175 to 300 °C. Each point on the graph corresponds to a new coupon etched for the denoted number of ALE cycles. Using new coupons for each experiment leads to some variance across multiple samples. However, the thickness change is approximately linear versus number of ALE cycles.

Cobalt etch rates from the results in Fig. 8 are plotted in Fig. 9. The smallest etch rate of 2.65 ± 0.35 Å/cycle is observed at 175 °C. The etch rates then increase with increasing temperature. Etch rates at 200, 225, 250, 275, and 300 °C are 2.95 ± 0.21, 3.39 ± 0.36, 5.47 ± 1.03, 7.06 ± 0.52, and 12.47 ± 2.40 Å/cycle, respectively. The error in the etch rates is from the variance between the different cobalt coupons.

The cobalt etch rates determined from the XRR measurements shown in Fig. 9 can be compared with the etch rates determined from the QCM studies displayed in Fig. 4. The etch rates at 175–275 °C are similar between the two methods. This similarity is notable because the cobalt films used in the QCM and XRR investigations were deposited using different deposition tools.

A discrepancy between the etch rates determined by the QCM and XRR investigations is observed at 300 °C. The QCM measurements shown in Fig. 4 observed a reduction in the cobalt etch rate at 300 °C. In contrast, the XRR measurements displayed in Fig. 9 observed an increase in the cobalt etch rate compared with the cobalt etch rate at 275 °C. One possible reason for this difference could be the different thicknesses of the cobalt films used in the two studies.

The initial cobalt film thickness on the QCM sensor was 200 nm. The cobalt surfaces were etched for hundreds of ALE cycles at 300 °C during the QCM experiments. Experiments were stopped after the cobalt thin film was reduced to around 50 nm. In contrast, the cobalt thin films studied by the XRR measurements had much smaller initial thicknesses of 13–17 nm. The cobalt films were completely removed by Co ALE in 15 cycles at 300 °C during the XRR experiments.

The longer experiments performed during the QCM measurements could result in the build-up of decomposition products on the surface. These decomposition products may explain the more scattered etching with the unexpectedly low etch rate at 300 °C in Fig. 4. In comparison, the time required for the XRR measurements was much shorter. There was much less time for decomposition products to accumulate and reduce the etch rate.

The etching of cobalt using SO_2Cl_2 and PMe_3 was also monitored using XRR measurements. Figure 10 shows the thickness change vs number of ALE cycles at 130, 150, and 175 °C. For these experiments, the number of individual PMe_3 exposures was fixed at 25 for each ALE cycle. Based on the QCM studies, 25 PMe_3 exposures should have been sufficient to remove the $CoCl_2$ surface layer at these temperatures. Each point on the graph corresponds with a new coupon etched for the designated number of ALE cycles. Using separate coupons for each XRR measurement leads to some variance. The variance is higher at higher temperatures as observed by the scatter in the individual measurements at 175 °C.

The observed cobalt etch rates using SO_2Cl_2 and PMe_3 as the reactants were 1.81 ± 0.13, 2.62 ± 0.29, and 2.51 ± 0.65 Å/cycle at 130, 150, and 175 °C, respectively. The error in the etch rates indicates that these three etch rates are not significantly different from each other. This trend versus temperature mirrors the cobalt etch rates displayed in Fig. 7 that were determined by QCM measurements with SO_2Cl_2 and PMe_3 as the reactants. These etch rates

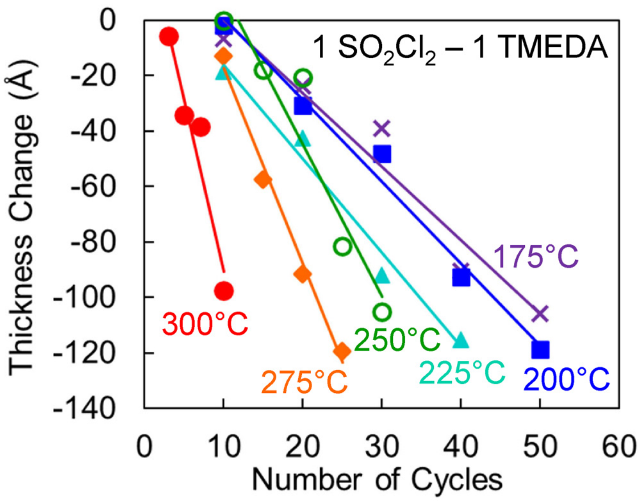

FIG. 8. Cobalt thickness change determined by XRR vs. number of SO_2Cl_2/TMEDA ALE cycles at 175, 200, 225, 250, 275, and 300 °C.

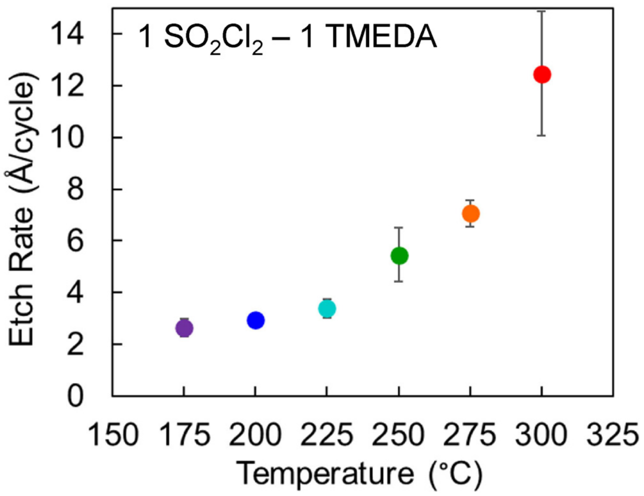

FIG. 9. Cobalt etch rates measured by XRR for Co ALE using the SO_2Cl_2/TMEDA process from 175 to 300 °C.

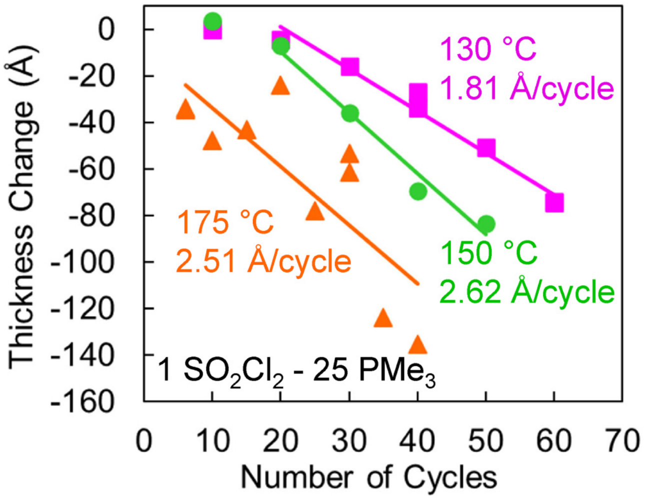

FIG. 10. Cobalt thickness change determined by XRR vs number of SO_2Cl_2/PMe_3 ALE cycles at 130, 150, and 175 °C.

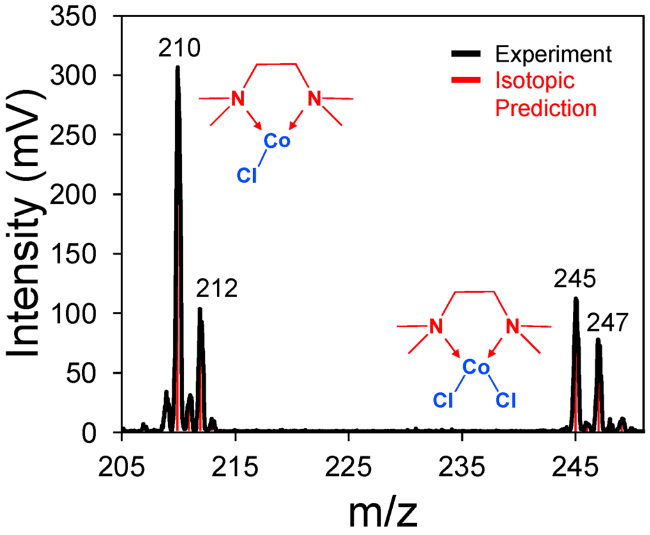

FIG. 11. Mass spectrometry results for $CoCl_2(TMEDA)^+$ from the cobalt etch product, $CoCl_2(TMEDA)$, and a cracking fragment, $CoCl(TMEDA)^+$, from the reaction of TMEDA with $CoCl_2$ powder at 250 °C.

were between 2 and 4 Å/cycle at all temperatures from 80 to 200 °C.

There is a slight etch delay at most temperatures for the XRR measurements using the individual cobalt coupons. This etch delay could be attributed to the native CoO layer on top of the cobalt film. The thickness of the CoO layer measured by XRR was typically ∼60–70 Å. This CoO layer must be removed from each cobalt coupon before measuring the underlying cobalt etching. In contrast, this native CoO layer can be removed prior to performing the various QCM measurements.

C. Quadrupole mass spectrometry studies

In situ QMS was utilized to identify the volatile etch products during Co thermal ALE. For the QMS experiments, the TMEDA reactant was flowed continuously over $CoCl_2$ powder.[35] The $CoCl_2$ powder mimics the cobalt surface after chlorination by SO_2Cl_2. The $CoCl_2$ powders also increase the sample surface area and maximize the intensity of the volatile etch products. There is a continuous etch product signal because the $CoCl_2$ powder is effectively an infinite reservoir. The etch product can be produced until the $CoCl_2$ powder is depleted.

Figure 11 shows the QMS results at 250 °C for the *m/z* window from 205 to 250 amu. Ion signals for $CoCl_2(TMEDA)^+$ from the $CoCl_2(TMEDA)$ etch product were observed in this *m/z* range. The major ion signals were monitored at *m/z* 245 and *m/z* 247. These ion signal intensities were in excellent agreement with the expected ion intensities based on the natural isotopic abundances of Cl and C. As mentioned earlier, $CoCl_2(TMEDA)$ is a documented Co compound.[37] $CoCl_2(TMEDA)$ has been used as a precursor for CoO ALD and the ALD of cobalt alloys at growth temperatures from 140 to 300 °C.[37–40]

The $CoCl_2(TMEDA)$ etch product is CoX_2L_2 using the notation from the covalent bond classification (CBC) method.[27] Earlier studies of Ni ALE using SO_2Cl_2 and PMe_3 observed $NiCl_2(PMe_3)_2$ as the etch product.[26,41] $NiCl_2(PMe_3)_2$ is NiX_2L_2 using the CBC method notation. NiX_2L_2 is a probable Ni compound according to the MLX plots of the CBC method.[42] In contrast, CoX_2L_2 is not a probable Co compound according to the MLX plots. The MLX plots predict CoL_4X (34%) and CoL_3X_3 (54%) as the most probable Co compounds.[42] This discrepancy indicates that the CBC method can help suggest possible X and L ligands to form stable etch products. However, the exact identity of these etch products may not be predicted by the MLX plots. The MLX plots reveal the probability of occurrence of various MLX complexes based on the known metal complexes reported in the *Dictionary of Organometallic Complexes*.[27]

Ion signals were also observed from $CoCl(TMEDA)^+$ in Fig. 11 with the major ion signals at *m/z* 210 and *m/z* 212. This ion signal is a fragment of $CoCl_2(TMEDA)^+$. $CoCl(TMEDA)^+$ can also be identified based on the Cl and C natural isotopic abundances. There is excellent agreement between the observed mass spectrum for $CoCl(TMEDA)^+$ and the calculated isotopic prediction.

The QMS studies also investigated the amount of volatile etch species observed at various $CoCl_2$ powder temperatures. Figure 12 shows the results during a temperature ramp from room temperature to 400 °C. During the temperature ramp, TMEDA was continuously flowed over the $CoCl_2$ powder. The molecular ions from $CoCl_2(TMEDA)$, its fragment, $CoCl(TMEDA)$, and TMEDA were monitored as a function of temperature.

The ion signals for $CoCl_2(TMEDA)^+$ and $CoCl(TMEDA)^+$ in Fig. 12(a) rise and fall with a prominent peak at 250 °C. The ion signals from TMEDA at *m/z* 116 and *m/z* 58 in Fig. 12(b) also rise and fall in a similar fashion with a peak at 250 °C. The ion signals from TMEDA are believed to be primarily from a fragment of the

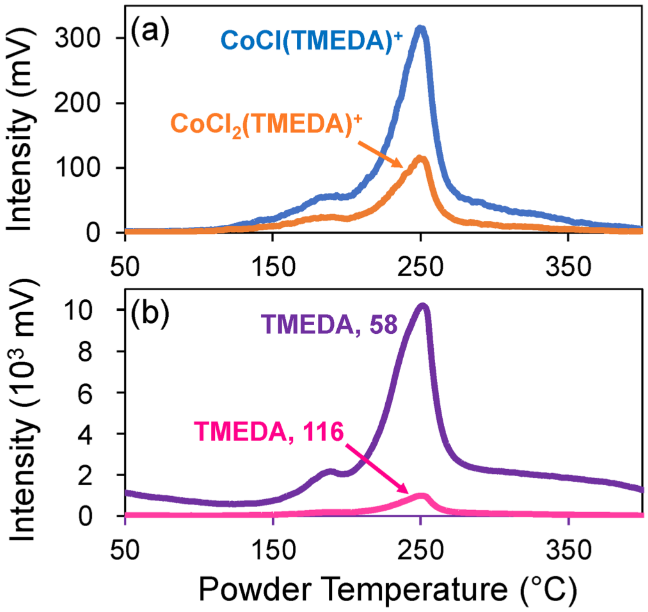

FIG. 12. Mass spectrometry results for ion intensities during the reaction of TMEDA with $CoCl_2$ powder. (a) Cobalt etch product, $CoCl_2(TMEDA)^+$, and main cracking fragment, $CoCl(TMEDA)^+$ vs $CoCl_2$ powder temperature. (b) TMEDA at *m/z* 116 and main cracking fragment of TMEDA at *m/z* 58 vs $CoCl_2$ powder temperature.

$CoCl_2(TMEDA)$ etch product. Some of the TMEDA ion signals are also from the continuous flow of the TMEDA precursor during the temperature ramp from 50 to 400 °C.

The $CoCl_2(TMEDA)^+$ ion signals are observed over the same temperature range from 175 to 300 °C where Co thermal ALE is observed by the QCM and XRR measurements. The QMS results cannot be directly compared with the Co ALE results because the QMS experiments use an infinite reservoir of $CoCl_2$ powder. The infinite reservoir of $CoCl_2$ may not be the same as the $CoCl_2$ surface layer on Co formed during the SO_2Cl_2 chlorination reaction. However, the observation of Co ALE together with the identification of the $CoCl_2(TMEDA)$ etch product from $CoCl_2$ powder from 175 to 300 °C helps to confirm the mechanism for Co thermal ALE shown in Fig. 1.

Figure 12 shows a distinctive peak at 250 °C during the continuous TMEDA flow at $CoCl_2$ powder temperatures from 50 to 400 °C. Similar peaks during temperature ramps have been observed for $NiCl_2(P(CH_3)_3)_2$ etch products from $P(CH_3)_3$ exposure on $NiCl_2$ powder, $PdCl_2(P(CH_3)_3)_2$ etch products from $P(CH_3)_3$ exposure on $PdCl_2$ powder, and $PtCl_2(P(CH_3)_3)_2$ etch products from $P(CH_3)_3$ exposure on $PtCl_2$ powder.[26,41] These peaks have been explained by the decreasing residence time for the $P(CH_3)_3$ precursor at higher temperatures.[26,41] The decreasing intensity for the etch products can be understood using a precursor-mediated adsorption model.[43]

QMS measurements during PMe_3 exposure on $CoCl_2$ powders did not observe Co etch products. Although Co etch products should be present, the intensity of these etch products may be much smaller because the ligand addition of PMe_3 to $CoCl_2$ is not efficient. As shown in Fig. 5, 30 PMe_3 individual exposures were required to remove the $CoCl_2$ surface layer. In contrast, one TMEDA exposure could remove the $CoCl_2$ surface layer as displayed in Fig. 2.

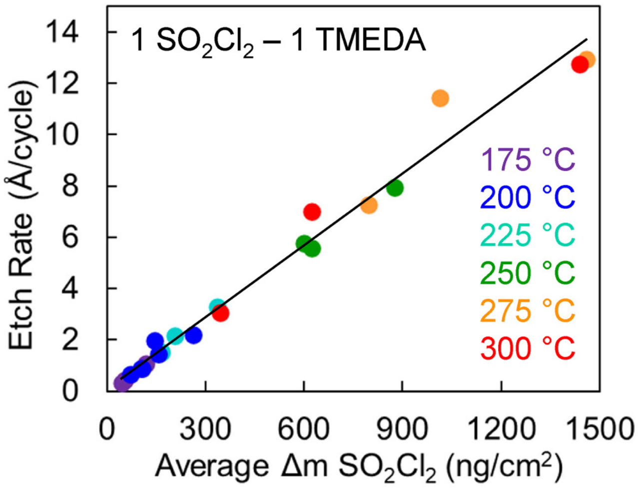

FIG. 13. Cobalt etch rates vs $\Delta m_{SO_2Cl_2}$ at various temperatures. These results indicate that cobalt etch rate is determined by the amount of cobalt chlorination.

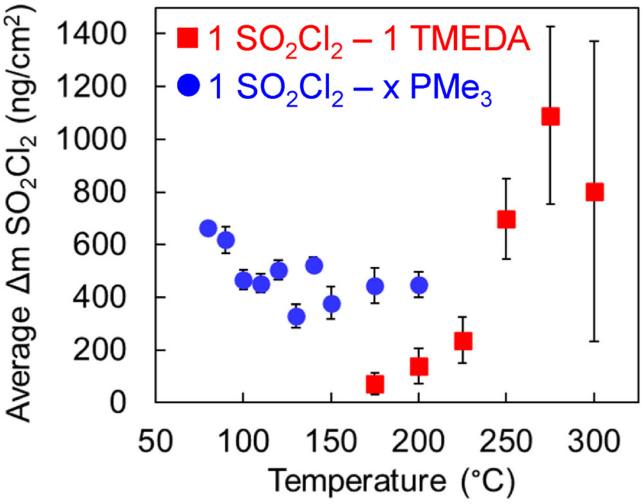

FIG. 14. Average $\Delta m_{SO_2Cl_2}$ vs temperature for Co ALE using the SO_2Cl_2/TMEDA process (red squares) and the SO_2Cl_2/PMe_3 ALE process (blue circles).

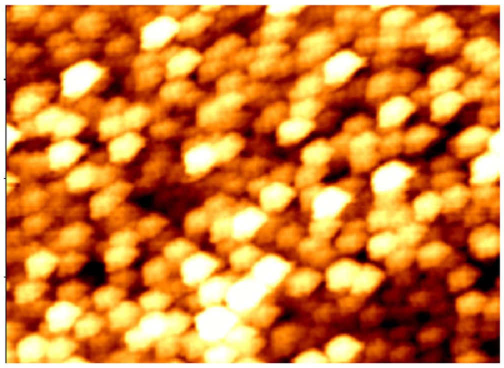

(a) Initial
R=1.62 nm

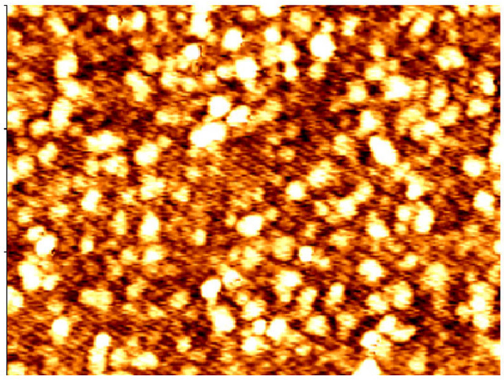

(b) 1 SO_2Cl_2/1 TMEDA
R=0.91 nm

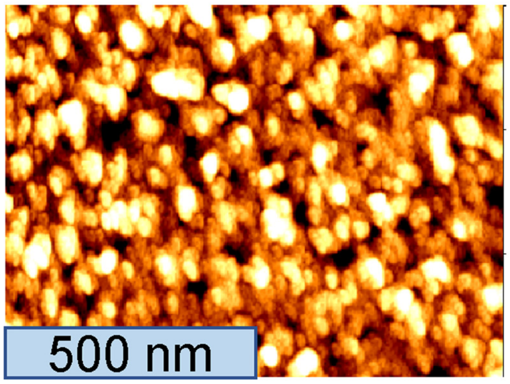

(c) 1 SO_2Cl_2/25 PMe_3
R=2.16 nm

FIG. 15. AFM images of (a) initial cobalt film; (b) cobalt film after 20 SO_2Cl_2/TMEDA cycles at 175°C; and (c) cobalt film after 40 SO_2Cl_2/PMe_3 cycles at 130 °C.

D. Mass change during SO_2Cl_2 exposure

Figure 13 shows the cobalt etch rate using SO_2Cl_2 and TMEDA as the reactants vs the average mass change during the SO_2Cl_2 exposure ($\Delta m_{SO_2Cl_2}$) during steady state etching. Each point represents the average $\Delta m_{SO_2Cl_2}$ from a separate QCM experiment. There were at least three experiments performed at each temperature. The plot shows a direct correlation between the cobalt etch rate and $\Delta m_{SO_2Cl_2}$. This correlation indicates that the cobalt etch rate is determined by the amount of $CoCl_2$ formed during the SO_2Cl_2 exposure when using SO_2Cl_2 and TMEDA as the reactants.

The cobalt etch rate vs temperature using SO_2Cl_2 and TMEDA as the reactants is shown in Fig. 4. The average $\Delta m_{SO_2Cl_2}$ vs temperature for the SO_2Cl_2/TMEDA etching process is displayed in Fig. 14. As expected given the results in Fig. 13, the average etch rate vs temperature in Fig. 4 and average $\Delta m_{SO_2Cl_2}$ vs temperature for TMEDA in Fig. 14 are nearly identical. In contrast, Fig. 14 shows that $\Delta m_{SO_2Cl_2}$ does not change significantly with temperature during the SO_2Cl_2 exposure with PMe_3 as the ligand-addition precursor. These results are consistent with the nearly constant cobalt etch rate vs temperature in Fig. 7 using SO_2Cl_2 and PMe_3 as the reactants.

The Co thermal ALE processes developed in this study were based on using one SO_2Cl_2 exposure for chlorination per ALE cycle. Additional SO_2Cl_2 exposures will lead to additional chlorination of the cobalt surface. Experiments that examined multiple SO_2Cl_2 exposures for cobalt chlorination are presented elsewhere.[45]

E. AFM measurements of surface roughness

AFM measurements were performed to determine the effect of Co thermal ALE on the surface roughness. Surface smoothing by ALE has been previously reported during the ALE of many materials such as Al_2O_3,[5,6,10] HfO_2,[44] and Si_3N_4.[19] The AFM measurements were conducted on cobalt films that were etched with SO_2Cl_2 and either TMEDA or PMe_3 as the ligand-exchange precursor. Figure 15 shows the AFM images before and after Co thermal ALE. The cobalt film before any Co ALE cycles had an initial RMS roughness of 1.62 nm.

After 20 cycles of SO_2Cl_2/TMEDA at 175 °C, the RMS roughness decreased to 0.91 nm. These 20 cycles removed 2.5 nm of the cobalt film. The RMS roughness of 0.91 nm indicates that the SO_2Cl_2/TMEDA etch process smoothed the cobalt film. In contrast, the SO_2Cl_2/PMe_3 etch process roughened the cobalt film. After 40 cycles at 130 °C, the RMS roughness was 2.16 nm. These 40 cycles removed 3 nm of the cobalt film.

Although the SO_2Cl_2/TMEDA and SO_2Cl_2/PMe_3 etch processes both removed approximately the same amount of the cobalt film, the SO_2Cl_2/TMEDA etch process at 175 °C smoothed the cobalt film and the SO_2Cl_2/PMe_3 process at 130 °C roughened the cobalt film. The difference could be attributed to the different temperatures for the two etch processes. The difference could also be caused by the multiple PMe_3 exposures required to remove the $CoCl_2$ layer during the SO_2Cl_2/PMe_3 process. Additional studies are required to understand these changes in surface roughness.

IV. CONCLUSIONS

A thermal ALE process for cobalt was developed using SO_2Cl_2 for chlorination and either TMEDA or PMe_3 for ligand-addition. QCM measurements observed a mass increase on every SO_2Cl_2 exposure and a mass decrease on every TMEDA or PMe_3 exposure. The average etch rates determined from QCM measurements for the SO_2Cl_2/TMEDA process at 175, 200, 225, 250, 275, and 300 °C were 0.62 ± 0.41, 1.35 ± 0.64, 2.31 ± 0.91, 6.43 ± 1.31, 10.56 ± 2.94, and 7.62 ± 4.87 Å/cycle, respectively. These Co etch rates were confirmed by XRR measurements using cobalt thin films on silicon coupons. In addition, the QCM measurements revealed that between 90% and 100% of the $CoCl_2$ surface layer formed during the SO_2Cl_2 exposure was removed during the TMEDA exposures.

In contrast, the SO_2Cl_2/PMe_3 process required 20–40 PMe_3 exposures to remove the $CoCl_2$ surface layer after each SO_2Cl_2 exposure at 130–200 °C. An increasing number of PMe_3 exposures were needed as the temperature decreased below 130 °C. The QCM and XRR measurements also revealed that the etch rates for the SO_2Cl_2/PMe_3 process were 2–4 Å/cycle and did not change with temperature. For both the SO_2Cl_2/TMEDA and SO_2Cl_2/PMe_3 processes, the Co etch rate was determined by the amount of $CoCl_2$ formed by the SO_2Cl_2 exposure. The thicker $CoCl_2$ surface layers during the SO_2Cl_2/TMEDA process at higher temperatures led to larger Co etch rates. In comparison, the SO_2Cl_2/PMe_3 process resulted in approximately the same amount of $CoCl_2$ formed at all temperatures and little dependence of the Co etch rate on temperature.

QMS analysis determined that the cobalt etch product during TMEDA exposures on $CoCl_2$ was $CoCl_2$(TMEDA). This Co etch product peaked at 250 °C and was observed over the same temperature range of 175–300 °C where etch rates were measured for Co thermal ALE. AFM measurements determined that the cobalt roughness decreased after ALE with the SO_2Cl_2/TMEDA process. In contrast, the cobalt surface roughness increased after Co ALE with the SO_2Cl_2/PMe_3 process. These results for Co thermal ALE using SO_2Cl_2 and either TMEDA or PMe_3 as the reactants add to the growing list of materials that can be etched by thermal ALE methods. The chlorination and ligand-addition mechanism for Co thermal ALE should be generally applicable for metal ALE for metals that form stable chlorides.

ACKNOWLEDGMENTS

This research was funded by Intel Corporation through a member specific research project administered by the Semiconductor Research Corporation. The authors acknowledge their Intel Liaisons (Eric Mattson, Scott Clendenning, Charles Mokhtarzadeh, and Jiun-Ruey Chen) for their helpful discussions. Funding for the QMS reactor and the QMS investigations was provided by Lam Research. The authors also acknowledge Charles Winter of Wayne State University for his useful suggestions regarding TMEDA.

AUTHOR DECLARATIONS

Conflict of Interest

The authors have no conflicts to disclose.

Author Contributions

Jessica A. Murdzek: Data curation (lead); Formal analysis (lead); Investigation (lead); Writing – original draft (lead); Writing – review & editing (equal). **Ann Lii-Rosales:** Data curation (supporting); Investigation (supporting). **Steven M. George:** Conceptualization (lead); Funding acquisition (lead); Methodology (lead); Project administration (lead); Supervision (lead); Writing – review & editing (equal).

DATA AVAILABILITY

The data that support the findings of this study are available within the article.

REFERENCES

[1] A. Fischer, A. Routzahn, S. M. George, and T. Lill, J. Vac. Sci. Technol. A **39**, 030801 (2021).

[2] S. M. George, Acc. Chem. Res. **53**, 1151 (2020).

[3] T. Faraz, F. Roozeboom, H. C. M. Knoops, and W. M. M. Kessels, ECS J. Solid State Sci. Technol. **4**, N5023 (2015).

[4] S. M. George, Chem. Rev. **110**, 111 (2010).

[5] Y. Lee and S. M. George, J. Phys. Chem. C **123**, 18455 (2019).

[6] D. R. Zywotko, J. Faguet, and S. M. George, J. Vac. Sci. Technol. A **36**, 061508 (2018).

[7] K. J. Kanarik, T. Lill, E. A. Hudson, S. Sriraman, S. Tan, J. Marks, V. Vahedi, and R. A. Gottscho, J. Vac. Sci. Technol. A **33**, 020802 (2015).

[8] A. M. Cano, A. E. Marquardt, J. W. DuMont, and S. M. George, J. Phys. Chem. C **123**, 10346 (2019).

[9] J. C. Gertsch, A. M. Cano, V. M. Bright, and S. M. George, Chem. Mater. **31**, 3624 (2019).

[10] Y. Lee and S. M. George, ACS Nano **9**, 2061 (2015).

[11] Y. Lee, J. W. DuMont, and S. M. George, Chem. Mater. **28**, 2994 (2016).

[12] Y. Lee and S. M. George, J. Vac. Sci. Technol. A **36**, 061504 (2018).

[13] J. A. Murdzek and S. M. George, J. Vac. Sci. Technol. A **38**, 022608 (2020).

[14] J. A. Murdzek, A. Rajashekhar, R. S. Makala, and S. M. George, J. Vac. Sci. Technol. A **39**, 042602 (2021).

[15] T. J. Myers, A. M. Cano, D. K. Lancaster, J. W. Clancey, and S. M. George, J. Vac. Sci. Technol. A **39**, 021001 (2021).

[16] J. W. DuMont, A. E. Marquardt, A. M. Cano, and S. M. George, ACS Appl. Mater. Interfaces **9**, 10296 (2017).

[17] N. R. Johnson and S. M. George, ACS Appl. Mater. Interfaces **9**, 34435 (2017).

[18] A. I. Abdulagatov and S. M. George, Chem. Mater. **30**, 8465 (2018).

[19] A. I. Abdulagatov and S. M. George, J. Vac. Sci. Technol. A **38**, 022607 (2020).

[20] A. I. Abdulagatov, V. Sharma, J. A. Murdzek, A. S. Cavanagh, and S. M. George, J. Vac. Sci. Technol. A **39**, 022602 (2021).

[21] Y. Lee and S. M. George, Chem. Mater. **29**, 8202 (2017).

[22] E. Mohimi, X. Q. I. Chu, B. B. Trinh, S. Babar, G. S. Girolami, and J. R. Abelson, ECS J. Solid State Sci. Technol. **7**, P491 (2018).

[23] M. Konh, C. He, X. Lin, X. Guo, V. Pallem, R. L. Opila, A. V. Teplyakov, Z. Wang, and B. Yuan, J. Vac. Sci. Technol. A **37**, 021004 (2019).

[24] Z. Wang and R. L. Opila, J. Vac. Sci. Technol. A **38**, 022611 (2020).

[25] S. Fujisaki, Y. Yamaguchi, H. Kobayashi, K. Shinoda, M. Yamada, H. Hamamura, K. Kawamura, and M. Izawa, Appl. Phys. Lett. **121**, 122102 (2022).

[26] J. A. Murdzek, A. Lii-Rosales, and S. M. George, Chem. Mater. **33**, 9174 (2021).

[27] M. L. H. Green, J. Organomet. Chem. **500**, 127 (1995).

[28] J. K. C. Chen, T. Kim, N. D. Altieri, E. Chen, and J. P. Chang, J. Vac. Sci. Technol. A **35**, 031304 (2017).

[29] J. E. Kim *et al.*, Nanotechnology **32**, 055301 (2021).

[30] A. Pacco, Y. Akanishi, Q. T. Le, E. Kesters, G. Murdoch, and F. Holsteyns, Microelectron. Eng. **217**, 111131 (2019).

[31] P. Walker and W. H. Tarn, *CRC Handbook of Metal Etchants* (CRC, Boca Raton, 1991).

[32] J. W. Elam, M. D. Groner, and S. M. George, Rev. Sci. Instrum. **73**, 2981 (2002).

[33] V. N. Moussa, Aust. J. Chem. **65**, 95 (2012).

[34] D. F. Smith, J. Am. Chem. Soc. **47**, 1862 (1925).

[35] A. Lii-Rosales, A. S. Cavanagh, A. Fischer, T. Lill, and S. M. George, Chem. Mater. **33**, 7719 (2021).

[36] HSC Chemistry, *HSC Chemistry 5.1* (Outokumpu Research Oy, Pori).

[37] K. Väyrynen, T. Hatanpää, M. Mattinen, M. Heikkilä, K. Mizohata, K. Meinander, J. Räisänen, M. Ritala, and M. Leskelä, Chem. Mater. **30**, 3499 (2018).

[38] H.-E. Nieminen, M. Kaipio, and M. Ritala, Chem. Mater. **32**, 8120 (2020).

[39] K. Väyrynen *et al.*, Adv. Mater. Interfaces **6**, 1801291 (2019).

[40] D. Zanders, J. Liu, J. Obenlüneschloß, C. Bock, D. Rogalla, L. Mai, M. Nolan, S. T. Barry, and A. Devi, Chem. Mater. **33**, 5045 (2021).

[41] A. Lii-Rosales, V. L. Johnson, S. Sharma, A. Fischer, T. Lill, and S. M. George, J. Phys. Chem. C **126**, 8287 (2022).

[42] See http://www.columbia.edu/cu/chemistry/groups/parkin/mlxz.htm for The Parkin Group, MLX Plots.

[43] D. A. King and M. G. Wells, Proc. R. Soc. London, Ser. A **339**, 245 (1974).

[44] Y. Lee, J. W. DuMont, and S. M. George, ECS J. Solid State Sci. Technol. **4**, N5013 (2015).

[45] See the supplementary material at https://www.scitation.org/doi/suppl/10.1116/6.0002488 for the description of experiments that explored cobalt chlorination using multiple SO_2Cl_2 exposures.